https://doi.org/10.18321/ectj1543

# Influence of Annealing Time on the Optical and Electrical Properties of Tin Dioxide-Based Coatings

**E.A. Dmitriyeva[1], I.A. Lebedev[1], E.A. Bondar[1]*, A.I. Fedosimova[1,2], S.A. Ibraimova[1], B.M. Nurbaev[1], A.S. Serikkanov[1], B.A. Baitimbetova[1]**

[1]Satbayev University, Institute of Physics and Technology, 22a Satbayev str., Almaty, Kazakhstan
[2]Institute of Nuclear Physics, 1 Ibragimov str., Almaty, Kazakhstan

**Article info**

Received:
30 May 2023

Received in revised form:
22 July 2023

Accepted:
26 August 2023

**Keywords:**
Tin dioxide, Electrical properties, Optical properties, Annealing, Transmission spectra, surface, Dendritic structures.

**Abstract**

This study investigates the effects of annealing time on the optical and electrical properties of tin dioxide coatings, specifically surface resistivity and specific conductivity. The thickness of the film, as well as its density and void density, were calculated from the interference peaks. The results suggest that as the duration of annealing increases, the density of the film decreases and the void volume increases. The lack of interference peaks in the transmission spectra of films containing additives is caused by the development of dendritic structures within the films. As the annealing duration is extended to 6 h, the surface resistivity increases, resulting in a decrease in the specific conductivity of all films. As the duration of annealing increases, the surface resistivity of the films studied increases and therefore their overall quality decreases.

## 1. Introduction

Tin dioxide stands out among a wide range of materials for optoelectronics [1, 2]. It is a semiconductor material with a unique characteristic of high optical transparency in the visible range of electromagnetic radiation and low electrical resistance [3, 4]. Tin dioxide has numerous applications, serving as a gas-trapping layer in various gas sensors [5, 6], an effective photoanode [7, 8], a protective coating against corrosion [9, 10], an antibacterial coating [11, 12], an anode for high-performance lithium-ion batteries [13, 14] and for various other purposes. Tin dioxide also has medical applications, such as serving as a glucose sensor [15, 16]. The broad range of properties exhibited by this semiconductor material [17, 18] enables it to be used in other applications too.

One promising area of energy is alternative energy sources [19–21], including wind energy [22–24] and solar energy [25–27]. Currently, solar cells have been widely adopted, being used in households and production, amongst others. However, difficulties exist with their usage, specifically regarding their reduced ability to absorb sunlight due to high surface reflection rates [28–30]. Efforts to enhance solar cell efficacy are of paramount importance. To minimize reflection coefficients, illuminating coatings come into play. For illuminating coatings for solar cells, thin nanostructured layers of tin dioxide are best suited [31]. It is noteworthy that annealing these coatings is essential to regulate their characteristics. The scientific task of determining the duration of their operation is a challenge.

The objective of this study was to investigate how annealing time influences the optical and electrical characteristics of tin dioxide coatings that were created from lyophilic and lyophobic film-forming systems.

## 2. Experimental

The synthesis of film-forming systems involved the following reagents: crystalline hydrate of tin tetrachloride pentahydrate $SnCl_4 \cdot 5H_2O$ (grade “pure”), purified ethyl alcohol $C_2H_5OH$ (corresponding to GOST 5962-2013. “Rectified ethyl alcohol from edible raw material. Specifications”), concentrated aqueous solution of ammonia $NH_4OH$ (grade “pure”), ammonium fluoride $NH_4F$ in as a dopant (qualified “pure for analysis”).

*Corresponding author.
E-mail address: bondar@sci.kz

A total of 5 film-forming systems were synthesized, of which:

*lyophilic:*

1) $SnCl_4$/EtOH: Tin tetrachloride crystalline hydrate was ground manually using a pestle and mortar to a powder. Then $SnCl_4 \cdot 5H_2O$ was dissolved in ethyl alcohol. The molarity of the system is 0.13 mol/L;

2) $SnCl_4$/EtOH/$NH_4F$: a dopant, $NH_4F$, was added to the $SnCl_4$/EtOH system. $NH_4F$ was dissolved in the system by stirring under parallel heating. The stirring time was 2 h, the rotation speed was 140 rpm, temperature was 35 °C. The ratio of $Sn^{4+}$ ions to $F^-$ ions was 10/4;

3) $SnCl_4$/EtOH/$NH_4OH$: an alcohol solution of ammonia was introduced into the $SnCl_4$/EtOH system. The ammonia concentration in the ammonia-alcohol mixture was 3.5 mol/L. At the same time, the pH of the system was 1.80, as in the $SnCl_4$/EtOH/$NH_4F$ system to be able to compare systems.

*lyophobic:*

4) $SnO_2$ in the form of a dispersed phase: an aqueous solution of ammonia was introduced into the $SnCl_4$/EtOH system until $Sn(OH)_2$ was completely precipitated. Next, heating with stirring was carried out: temperature is 100 °C, speed is 160 rpm to remove the solvent and decompose $Sn(OH)_2$ to $SnO_2$ and $H_2O$. The result is a white tin oxide powder. The powder was transferred into a suspension with ethyl alcohol at a stirring speed of 100 rpm for 4 h. The $SnO_2$ concentration in the resulting system was 0.13 mol/L.

5) $SnO_2$ in the form of a dispersed phase with $NH_4F$: the $NH_4F$ dopant was introduced into lyophobic system No. 4. The ratio of $Sn^{4+}$ ions to $F^-$ ions was 10/4.

To deposit the synthesized film-forming systems, glass slides were used that had previously undergone a cleaning procedure. The systems were deposited by spin-coating. The rotation speed was 3000 rpm, and the time was 3–5 s. Next, the samples underwent a drying procedure under infrared radiation at a temperature of 80 °C for 1–2 min. Annealing was carried out in a muffle furnace at a temperature of 400 °C for 15 min. The samples were cooled under air and the process was then repeated. The total number of applied layers is 15.

Film thickness was determined using the microweighing method. When calculating the film thickness, the following formula was used:

$$d = \frac{m_{sample} - m_{subst}}{\rho_{cass} \cdot S_{subst}} \quad (1)$$

where $d$ is the thickness of the film, $m_{sample}$ is the mass of the sample, $m_{sub}$ is the mass of the glass substrate, $\rho_{cass}$ is the density of cassiterite taken as 7.0 g/cm$^3$, $S_{subst}$ is the area of the glass substrate.

The thicknesses of the film varied depending on the composition of the film-forming system: 250±7 nm for $SnCl_4$/EtOH; 152±7 nm for $SnCl_4$/EtOH/$NH_4F$; 193±7 nm for $SnCl_4$/EtOH/$NH_4OH$; 60±7 nm for $SnO_2$ in the form of a dispersed phase; 90±7 nm for $SnO_2$ in the form of a dispersed phase with $NH_4F$.

Surface resistivity was measured using a four-probe method.

The acidity of the systems was evaluated using a pH meter «pH-150M».

Optical characteristics (transmission and absorption spectra) of the samples were determined using a UNICO 2800 spectrophotometer.

The synthesized samples underwent annealing for 15 min, 3 h, and 6 h at 400 °C in a muffle furnace.

## 3. Results and discussion

Figure 1 shows the transmission spectra of films obtained from the $SnCl_4$/EtOH film-forming system.

It is evident from Fig. 1 that extending the annealing period results in a rise in the transmittance of the films.

The film thickness was calculated from the available interference peaks.

The density of the film was determined by using the disparity in the film thickness measured via micro-weighing and from the transmission spectra.

$$\rho_{opt} = \frac{m}{V} = \frac{\rho_{cass} * S_{subst} * d_{weig}}{S_{subst} * d_{opt}} = \frac{\rho_{cass} * d_{weig}}{d_{opt}} \quad (2)$$

where $\rho_{opt}$ is film density calculated from transmission spectra, $m$ is film mass, $V$ is film volume, $d_{weig}$ is film thickness obtained by microweighing method, $d_{opt}$ is film thickness calculated from the conditions of interference extrema.

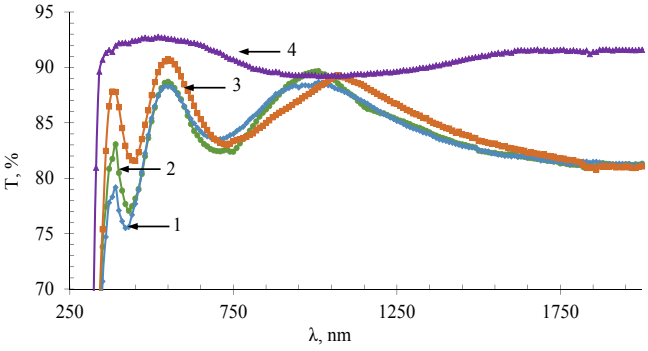


**Fig. 1.** Transmission spectra of films obtained from the $SnCl_4$/EtOH film-forming system: 1 – 15 min annealing; 2 – 3 h annealing, 3 – 6 h annealing, 4 – glass substrate.

The voids were calculated based on the disparity in density between the film and cassiterite. The density of cassiterite is equivalent to that of a single $SnO_2$ crystal, while the film consists of $SnO_2$ crystallites and interstitial voids.

$$V_{void} = \frac{\rho_{cass} - \rho_{opt}}{\rho_{cass}} * 100\% \quad (3)$$

where, $V_{void}$ is void volume (%).

Extinction coefficients at extremum points were determined. The calculation results are presented in Table 1.

Table 1 illustrates that the thickness of the film rises with longer annealing periods. Consequently, the density of the film decreases, while voids increase. The increase in voids may improve sensitivity to gases due to the higher number of adsorption-desorption centers. Additionally, the extinction coefficient descends with a more prolonged annealing duration.

Figure 2 shows the transmission spectra of films obtained from film-forming systems: $SnCl_4$/EtOH/$NH_4F$, $SnCl_4$/EtOH/$NH_4OH$, $SnO_2$ in the form of a dispersed phase, and $SnO_2$ in the form of a dispersed phase with $NH_4F$, after annealing for 3 and 6 h.

Figure 2 (a) demonstrates a decrease in the transmittance of films from the $SnCl_4$/EtOH/$NH_4F$ film-forming system in the visible region of the spectrum following annealing, while Fig. 2 (b) reveals that the transmittance of films from the $SnCl_4$/EtOH/$NH_4OH$ film-forming system is barely affected even after 6 h of annealing. Films synthesized from a $SnO_2$ dispersed phase system without additives, as well as those with the addition of $NH_4F$ after annealing at 400 °C for 15 min, exhibit transparency of 70–80% for wavelengths ranging from 550–2300 nm (Fig. 2 (c)

**Table 1.** Calculated film parameters.

| Annealing time | Thickness in nm | Density, g/cm$^3$ | $V_{void}$, % | k, λ=380 | k, λ=450 | k, λ=550 |
|---|---|---|---|---|---|---|
| 15 min | 313 | 5.59 | 20 | 0.023 | 0.031 | 0.017 |
| 3 h | 317 | 5.52 | 21 | 0.018 | 0.028 | 0.016 |
| 6 h | 330 | 5.30 | 24 | 0.012 | 0.022 | 0.013 |

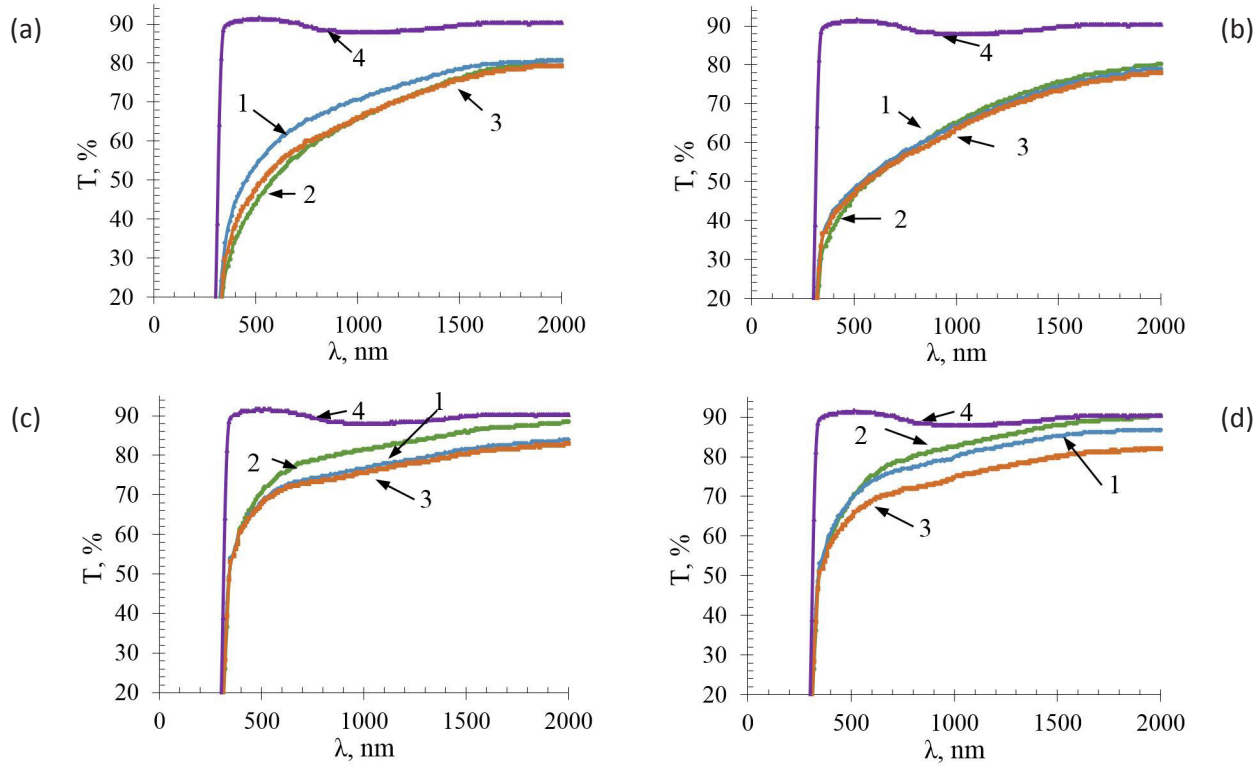


**Fig. 2.** Transmission spectra of films after annealing: (a) – $SnCl_4$/EtOH/$NH_4F$; (b) – $SnCl_4$/EtOH/$NH_4OH$; (c) – $SnO_2$ as a dispersed phase; (d) – $SnO_2$ as a dispersed phase with $NH_4F$.
1 – 15 min annealing, 2 – 3 h annealing, 3 – 6 h annealing, 4 – glass substrate.

and (d)). Following annealing at 400 °C for a duration of 3 h, there is an up to 7% enhancement in transparency within the same wavelength range. Such a boost in transparency may result from a reduction in structural defects. Further annealing for up to 6 h results in a reduction in film transparency obtained from a film-forming system containing $SnO_2$ as a dispersed phase without additives, to equivalent values seen during annealing at 400 °C for 15 min (Fig. 2 (c), curves 1 and 3).

Annealing of films obtained from a film-forming system containing $SnO_2$ in the form of a dispersed phase with the addition of $NH_4F$ at 400 °C for up to 6 h leads to a decrease in transparency for wavelengths of 550–2300 nm to 66–82% (Fig. 2(d), curve 3).

A decrease in film transparency may occur as the annealing duration increases by up to 6 hours. This decrease may be linked to the rise of heterogeneity in the film structure, as well as the emergence of microcracks and other defects [32].

Figure 3 shows SEM images of the film surface. The films, except for those produced from the $SnCl_4$/EtOH film-forming system, display various dendritic structures [33, 34]. The lack of interference peaks in the transmission spectra can be attributed to the scattering of electromagnetic radiation by surface irregularities on the films. During the annealing process, no significant changes in the film surface were detected.

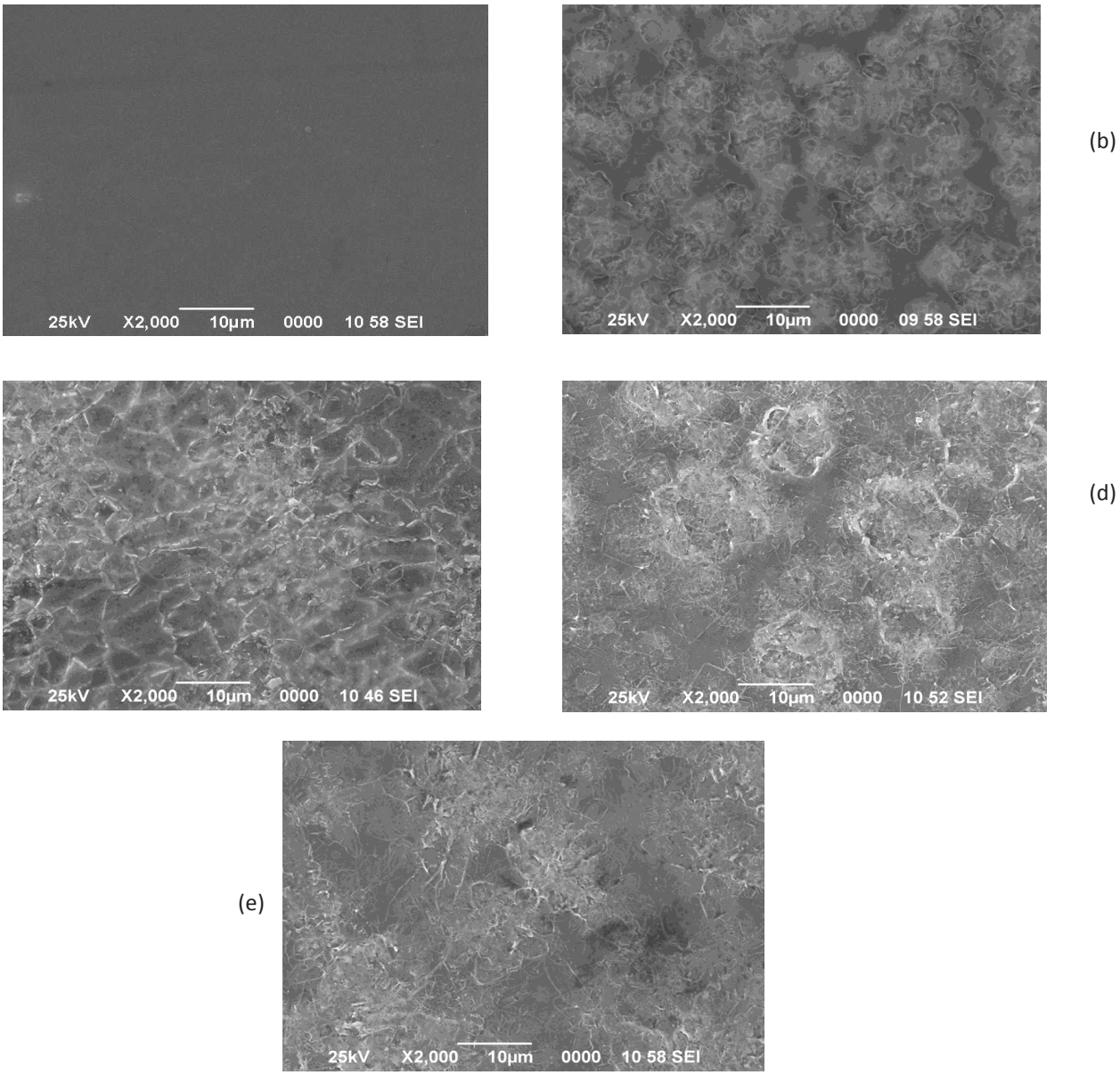


**Fig. 3.** SEM images of film surfaces. Composition of film-forming systems: (a) – $SnCl_4$/EtOH; (b) – $SnCl_4$/EtOH/$NH_4F$; (c) – $SnCl_4$/EtOH/$NH_4OH$; (d) – $SnO_2$ as a dispersed phase; (e) – $SnO_2$ as a dispersed phase with $NH_4F$.

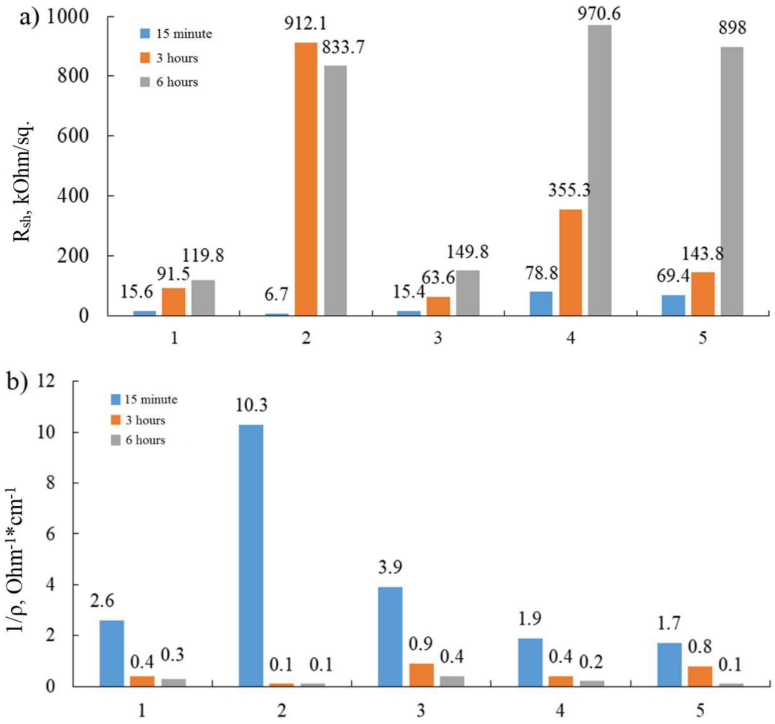


**Fig. 4.** (a) – surface resistance; (b) – conductivity. Composition of film-forming systems: (1) $SnCl_4$/EtOH; (2) $SnCl_4$/EtOH/$NH_4F$; (3) $SnCl_4$/EtOH/$NH_4OH$; (4) $SnO_2$ in the form of a dispersed phase; (5) $SnO_2$ in the form of a dispersed phase with $NH_4F$.

Figure 4 shows the change in the values of surface resistance and conductivity of the films depending on the duration of annealing.

It is evident from Fig. 4 that prolonging the annealing duration to 6 h results in an increase in surface resistance, which consequently leads to a decline in the conductivity of all films. This could be owing to reducing the charge carriers' free path. However, films obtained from the $SnCl_4$/EtOH/$NH_4F$ system display an increase in surface resistance by multiple magnitudes after 3 h of annealing. It is assumed that when films formed utilizing $NH_4F$-containing film-forming systems are developed, certain fluorine ions can become part of the film structure by adhering to tin ions, while others develop separate $NH_4F$ crystallites which decompose in two stages upon being heated [35, 36].

1st stage. At 167 °C, ammonium fluoride decomposes into gaseous ammonia ($NH_3$) and ammonium hydrofluoride ($NH_4HF_2$) according to the reaction:

$$2NH_4F \xrightarrow{>167\ ^\circ C} NH_4(HF_2) + NH_3\uparrow \qquad (4)$$

2nd stage. At 238 °C, ammonium hydrofluoride decomposes into ammonia gas ($NH_3$) and hydrogen fluoride gas (HF) according to the reaction:

$$NH_4(HF_2) \xrightarrow{>238\ ^\circ C} NH_3\uparrow + 2HF\uparrow \qquad (5)$$

Since the annealing temperature of the samples is 400 °C higher than the decomposition temperature of $NH_4F$, voids are formed in place of ammonium fluoride crystallites.

Increasing annealing to 6 h for these films leads to a decrease in surface resistance compared to 3-hour annealing. Presumably due to the annealing of small defects left after the decomposition of $NH_4F$.

One potential application of films made from tin oxide is in the production of transparent conductive coatings. In such cases, it is crucial to take into account both transmittance and surface resistance. The quality factor, determined by the Haacke relation [37, 38], provides a means for assessing the quality of the resulting films:

$$\Phi = (T/100)^{10}/R_{sh}, \qquad (6)$$

where Φ is the quality factor, $T$ and $R_{sh}$ are the transmittance and surface resistance of the film, respectively. When calculating the quality factor, the average transmittance for the visible wavelength range was taken.

Table 2 shows the values of the average transmittance in the wavelength range from 400 nm to 700 nm and the quality factor of the films. Table 2 reveals that films produced from the $SnCl_4$/EtOH film-forming system obtain the highest transmit-

**Table 2.** Average transmittance and quality factor.

| Composition of the film-forming system | $T_{av}$, % λ = 400–700 nm | | | Φ, $10^{-7}$ $Ohm^{-1}$ | | |
|---|---|---|---|---|---|---|
| | 15 min | 3 h | 6 h | 15 min | 3 h | 6 h |
| $SnCl_4$/EtOH | 86.3 | 86.4 | 89.1 | 146.8 | 25.4 | 26.4 |
| $SnCl_4$/EtOH/$NH_4F$ | 57.9 | 48.6 | 51.9 | 6.3 | 0.008 | 0.017 |
| $SnCl_4$/EtOH/NH4OH | 51.7 | 49.7 | 50.6 | 0.9 | 0.14 | 0.072 |
| $SnO_2$ as a dispersed phase | 71.6 | 74.6 | 71.0 | 4.5 | 1.5 | 0.3 |
| $SnO_2$ as a dispersed phase with $NH_4F$ | 73.0 | 73.6 | 68.3 | 6.2 | 3.24 | 0.2 |

tance of 89.1% in the visible region of the spectrum after a 6 h annealing process. Nevertheless, after the 6 h annealing process, the quality factor of these films reduces due to an increase in surface resistance. Thus, the quality factor of all the studied films reduces with the duration of annealing because of the rise in surface resistance. Of the films studied, those produced by the $SnCl_4$/EtOH film-forming method and subjected to 15 min of annealing showed superior quality factors.

## 4. Conclusion

The experiment results demonstrate that increasing the annealing duration leads to higher transmittance in films synthesized from the $SnCl_4$/EtOH film-forming method. However, the transmittance of samples obtained from the $SnCl_4$/EtOH/$NH_4OH$ system displays minimal change during an increase in annealing duration. As a result, the films exhibit a reduced density and increased void volume. The $SnCl_4$/EtOH/$NH_4OH$ film-forming system is rendered more appealing for the advancement and exploration of transparent coatings that are subjected to enduring thermal effects. Upon annealing at 400 °C for up to 6 h, the surface resistance of the films increases due to the reduction in the free path of charge carriers.

## Acknowledgment

The research was financially supported by the Science Committee of the Ministry of Education and Science of the Republic of Kazakhstan under the BR21881954 program.

## References

[1]. D.O. Murzalinov, A.A. Shaikenova, A.G. Umirzakov, A.I. Fedosimova, et al., *J. Phys.: Conf. Ser.* 2155 (2022) 012008. DOI: 10.1088/1742-6596/2155/1/012008

[2]. J.Y. Huang, G.S. Huang, Z. Zhao, C. Wang, et al., *J. Phys.: Condens. Matter* 35 (2023) 093001. DOI: 10.1088/1361-648X/acabf3

[3]. T.M.W.J. Bandara, A.A.A.P. Aththanayake, G.R.A. Kumara, P. Samarasekara, et al., *MRS Advances* 6 (2021) 417–421. DOI: 10.1557/s43580-021-00017-0

[4]. N.M. Tompakova, A.A. Polisan, *Russ. Microelectron.* 50 (2020) 679–687. DOI: 10.1134/S1063739721080126

[5]. G. Domènech-Gil, J. Samà, C. Fàbrega, I. Gràcia, et al., *Sens. Actuators B: Chem.* 383 (2023) 133545. DOI: 10.1016/j.snb.2023.133545

[6]. E.A. Grushevskaya, S.A. Ibraimova, E.A. Dmitriyeva, I.A. Lebedev, et al., *Eurasian Chem.-Technol. J.* 21 (2019) 13–17. DOI: 10.18321/ectj781

[7]. A.S. Altowyan, M. Shaban, K. Abdelkarem, A.M. El Sayed, *Materials* 15 (2022) 6534. DOI: 10.3390/ma15196534

[8]. S. Kahng, J.H. Kim, *Chemosphere* 291 (2022) 132800. DOI: 10.1016/j.chemosphere.2021.132800

[9]. J. Zhu, J. Han, W. Yu, N. Geng, et al., *Int. J. Electrochem. Sci.* 17 (2022) 221054. DOI: 10.20964/2022.10.53

[10]. J.K. Malav, R. Rathod, S. Umare, A. Patil, S. Ghugal, *Mater. Res. Express* 6 (2019) 065306. DOI: 10.1088/2053-1591/ab0925

[11]. S. Abirami, G. Viruthagiri, K. Ashokkumar, *Mater. Today: Proc.* 73 (2023) 535–538. DOI: 10.1016/j.matpr.2022.11.442

[12]. T. Amutha, M. Rameshbabu, M. Razia, Marwah Bakri, et al., *Spectrochim. Acta Part A: Mol. Biomol. Spectrosc.* 287 (2023) 121996. DOI: 10.1016/j.saa.2022.121996

[13]. S.S. Rasouli, P. Najafisayar, R. Hessam, *J. Electron. Mater.* 52 (2023) 896–906. DOI: 10.1007/s11664-022-10102-1

[14]. Y. Xin, S. Pan, X. Hu, C. Miao, et al., *J. Colloid Interface Sci.* 639 (2023) 133–144. DOI: 10.1016/j.jcis.2023.02.065

[15]. A.J. Haider, A.J. Mohammed, S.S. Shaker, K.Z. Yahya, M.J. Haider, *Energy Procedia* 119 (2017) 473-481. DOI: 10.1016/j.egypro.2017.07.056

[16]. S. Chatterjee, A.K. Pandey, "Plasmonic Sensor Utilizing Oxide and Antemonene Heterojunction for Glucose Sensing," 2022 Workshop on Recent Advances in Photonics, Mumbai, India, 2022, pp. 1–2. DOI: 10.1109/WRAP54064.2022.9758197
[17]. D.M. Mukhamedshina, A.I. Fedosimova, E.A. Dmitriyeva, I.A. Lebedev, et al., *Eurasian Chem.-Technol. J.* 21 (2019) 57–61. DOI: 10.18321/ectj791
[18]. A.F. Gouveia, C.M. Aldao, M.A. Ponce, E.R. Leite, E. Longo, *J. Andrés, Appl. Surf. Sci.* 622 (2023) 156904. DOI: 10.1016/j.apsusc.2023.156904
[19]. C.M. Sufyana, F.T. Akbar, W. Srigutomo, *Geotherm. Energy* 11 (2023). DOI: 10.1186/s40517-023-00249-3
[20]. H. Liang, F. You, *Nat. Commun.* 14 (2023) 1274. DOI: 10.1038/s41467-023-36827-z
[21]. S. Estévez, R. Rebolledo-Leiva, D. Hernández, S. González-García, et al., *Energy* 274 (2023) 127319. DOI: 10.1016/j.energy.2023.127319
[22]. J. Zoucha, C. Crespo, H. Wolf, M. Aboy, *Recent Pat. Eng.* 17 (2023) 3–15. DOI: 10.2174/1872212117666220829143132
[23]. Zhong yuan You, X. Wang, F. Lu, S. Wang, et al., *Nano Energy* 109 (2023) 108302. DOI: 10.1016/j.nanoen.2023.108302
[24]. S. Usha, M.S. Abishake, G. Anbezhil, S. Dhanasekar, *Mater. Today: Proc.* 72 (2023) 3075–3080. DOI: 10.1016/j.matpr.2022.09.250
[25]. B. Ghaleb, S.S. Abbasi, M. Asif, *Energy Rep.* 9 (2023) 3932–3942. DOI: 10.1016/j.egyr.2023.02.085
[26]. T. Nie, Z. Fang, X. Ren, Y. Duan, S. Liu, *Nano-Micro Lett.* 15 (2023) 70. DOI: 10.1007/s40820-023-01040-6
[27]. J. Kaiprath, V.V. Kishor Kumar, *Int. J. Air-Cond. Ref.* 31 (2023) 6. DOI: 10.1007/s44189-023-00022-y
[28]. A. Melliti, *Optik* 281 (2023) 170837. DOI: 10.1016/j.ijleo.2023.170837
[29]. M. Raja Nayak, B. Balaji, V. Charitha Sri, S. Pavan Kalyan, *AIP Conf. Proc.* 2452 (2022) 090006. DOI: 10.1063/5.0113217
[30]. A.M. El-Mahalawy, F.M. Amin, A.R. Wassel, M. Abd-El Salam, *J. Alloys Compd.* 923 (2022) 166484. DOI: 10.1016/j.jallcom.2022.166484
[31]. El M. Bouabdalli, M. El Jouad, T. Garmim, A. Louardi, et al., *Mater. Sci. Eng. B: Solid-State Mater. Adv. Technol.* 286 (2022) 116044. DOI: 10.1016/j.mseb.2022.116044
[32]. E.A. Dmitriyeva, E.A. Grushevskaya, D.M. Mukhamedshina, K.A. Mit, I.A. Lebedev, *Rec. Contr. Phys.* 72 (2020) 81–88. DOI: 10.26577/RCPh.2020.v72.i1.10 (in Russ.)
[33]. Ruohong Sui, Paul A. Charpentier, Robert A. Marriott, *Nanomaterials* 11 (2021) 1686. DOI: 10.3390/nano11071686
[34]. M. Zasadzinska, T. Knych, B. Smyrak, P. Strzepek, *Materials* 13 (2020) 5513. DOI: 10.3390/ma13235513
[35]. R.I. Kraydenko, Fluoroammonium separation of multicomponent silicate systems into individual oxides 05.17.02. – Technology of rare, scattered and radioactive elements. Abstract of the dissertation for the degree of candidate of chemical sciences. Tomsk, 2008, p. 2. (in Russ.)
[36]. A.A. Smorokov, A.S. Kantaev, V.A. Borisov, *AIP Conf. Proc.* 2143 (2019) 020022. DOI: 10.1063/1.5122921
[37]. A. Tarighi, A. Mashreghi, *J. Electron. Mater.* 48 (2019) 7827–7835. DOI: 10.1007/s11664-019-07622-8.
[38]. H. Miranda, S. Velumani, C.A. Samudio Pérez, J.C. Krause, et al., *J. Mater. Sci.: Mater. Electron.* 30 (2019) 15563–15581. DOI: 10.1007/s10854-019-01933-6